

The Frequency Dependence of the Conductivity and Dielectric Relaxation of $[(\text{CH}_2)_3(\text{NH}_3)_2]\text{Cu}(\text{II})\text{Cl}_4$

Mohga F. Mostafa, Ahmed A. A. Youssef, Samy S. Montasser, and Shaima S. Khyami

Physics Department, Faculty of Science, University of Cairo, Giza, Egypt

Reprint requests to Dr. M. F. M.; E-mail: Mohga40@yahoo.com

Z. Naturforsch. **60a**, 837 – 847 (2005); received October 7, 2005

The structural, dielectric and conductive properties of $[(\text{CH}_2)_3(\text{NH}_3)_2]\text{Cu}(\text{II})\text{Cl}_4$ have been studied. The material shows an order-disorder transition at $T_1 = (333 \pm 2)$ K and a ferroelectric phase transitions at $T_2 = (434 \pm 3)$ K. Results of differential thermal analysis, infrared spectroscopy, X-ray diffraction, AC conductivity and permittivity measurements are reported and discussed. The conductivity results are interpreted in terms of barrier hopping at low and intermediate temperatures, and band-type conduction at high temperatures. – PACS: 81.05.-t, 77.22.-d

Key words: Ferroelectrics; Dielectric Response; Transport Properties.

1. Introduction

Compounds of the series $[(\text{CH}_2)_n(\text{NH}_3)_2]\text{MCl}_4$, $\text{M} = \text{Mn, Fe, and Cu}$, $n = 2, 3, \dots$ have been intensively investigated because of their interesting magnetic properties. They undergo two-dimensional magnetic ordering at low temperatures [1–5]. More recently, studies of the Mn, Fe and Cd compounds showed interesting structural phase changes, which are reflected by their electric properties, particularly at higher temperatures [7–8]. Few studies regarding the electric properties in the high temperature range have been carried out on compounds containing Cu, although such studies would be interesting, as Cu compounds are known to show strong Jahn-Teller distortion. Long-chain ($n > 5$) salts, where $\text{M} = \text{Cu}$ and $n = 9$ and 12, have been studied in our laboratory [9, 10]. They are characterized by chain melting transitions [7]. The two Cu salts showed three phase transitions: two consecutive transitions near ambient temperature, which were attributed to chain melting, and a transition near $T \sim 380$ K, which possesses a large entropy that may be associated with an order-disorder phase change. Some of the short-chain ($n \leq 5$) metal complexes, such as $[(\text{CH}_2)_3(\text{NH}_3)_2]\text{MnCl}_4$ and $[(\text{CH}_2)_3(\text{NH}_3)_2]\text{CdCl}_4$, showed structural transformations. The former has two transitions at 305 and 337 K, the latter only one transition at 374 K from an antiferroelectric to a paraelectric phase. No transitions were reported for all metal complexes with $n = 2$ in

the temperature range between 4 K and its decomposition temperature [11, 12]. Thus it is of interest to investigate the phase changes of $[(\text{CH}_2)_3(\text{NH}_3)_2]\text{CuCl}_4$. X-ray investigation of this compound has indicated that it is isomorphous with the corresponding Cd salt, and that it crystallizes in the orthorhombic space group $Pnma$ with four formula units in a cell of the dimensions $a = 7.200(2)$ Å, $b = 18.247(7)$ Å and $c = 7.451(2)$ Å [13]. The structure consists of tetragonally distorted $[\text{CuCl}_4]^{2-}$ units which are chloro-bridged to form two-dimensional layers. Within this network there are two short Cu-Cl bond distances of 2.275(4) Å and two long Cu-Cl distances of 2.947(4) Å. There are two Cu-Cl bonds nearly perpendicular to the bridged layer with distances of 2.314(4) Å. The chlorocuprate sheet is puckered due to the hydrogen bonding to the propylene-1,3-diammonium ions which lie between the layers.

In this paper, differential thermal analysis and permittivity measurements at $300 \text{ K} < T < 450 \text{ K}$ in the frequency range 100 Hz – 100 kHz are reported. IR, X-ray and chemical analyses were carried out to confirm the formation of the material.

2. Experimental

The sample was prepared as described in [14]. The yellow sample of $[(\text{CH}_2)_3(\text{NH}_3)_2]\text{CuCl}_4$, denoted C3Cu, was recrystallized from a mixture of alcohol and diethyl ether and then dried in vacuum. The results of the chemical analysis are listed in Table 1.

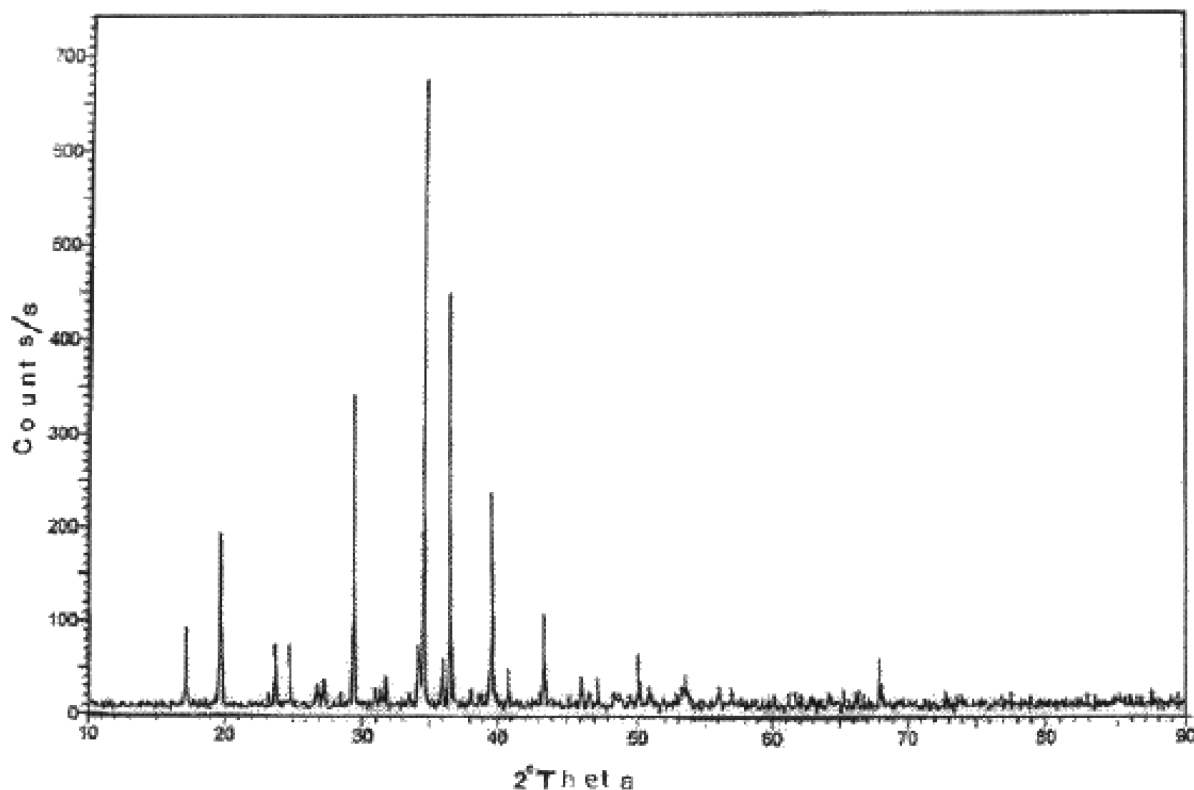


Fig. 1. X-ray diffraction pattern at 297 K of the sample C3Cu.

Table 1. Results of the chemical analysis of $[(\text{CH}_2)_3(\text{NH}_3)_2]\text{CuCl}_4$.

	C	H	N	Cl	Cu
Calcd. (%)	12.79	4.273	9.947	50.44	22.57
Found (%)	11.99	4.07	9.75	49.1	22.75

Table 2. Wave number (cm^{-1}) of IR bands and their assignment of $(\text{CH}_2)_3(\text{NH}_3)_2\text{Cl}_2$ and $[(\text{CH}_2)_3(\text{NH}_3)_2]\text{CuCl}_4$ at room temperature.

$(\text{CH}_2)_3(\text{NH}_3)_2\text{Cl}_2$	$[(\text{CH}_2)_3(\text{NH}_3)_2]\text{CuCl}_4$	Band assignment
1599, 1475	1583, 1487	NH_3 def.
1187, 1102	1185, 1102	CH_2 wagg./ $(\text{NH}_3)^+/\text{C-H}$ str.
943, 780	939	CH_2 rocking
	278, 235	Cu-Cl str. and Cu-Cl layer

The IR spectrum between 4000 cm^{-1} and 200 cm^{-1} was obtained using an FTIR 5000 spectrometer at Mansoura University. The bands and their assignment are listed in Table 2.

The X-ray diffraction of the powder at room temperature was obtained using a Siemens (D5000) diffractometer (Ni filtered $\text{Cu-K}\alpha$ radiation), wave length

1.54057 \AA . A film of uniform thickness was used. Scans were recorded for every 0.05° step from $2\theta = 10^\circ - 90^\circ$ at $T = 297 \text{ K}$.

The complex dielectric permittivity ϵ^* in the frequency range $60 \text{ Hz} - 100 \text{ kHz}$ was measured using a computer controlled lock-in amplifier type PAR 5207. The temperature was measured with a copper constantan thermocouple. The samples were 8.0 mm in diameter and 1.0 mm thick. The surfaces were coated with silver paste to ensure good electrical contact. Different samples were used. The results were reproducible. The measurements were carried out while heating.

3. Results and Discussion

3.1. Structure and Thermal Behavior

Figure 1 shows the X-ray diffraction pattern at 297 K of the sample C3Cu. The diffraction lines correspond to the orthorhombic space group $Pnma$ with the lattice spacing: $a = 7.20 \text{ \AA}$, $b = 18.247 \text{ \AA}$ and $c = 7.451 \text{ \AA}$. They agree with the results of Phelps *et al.* [13].

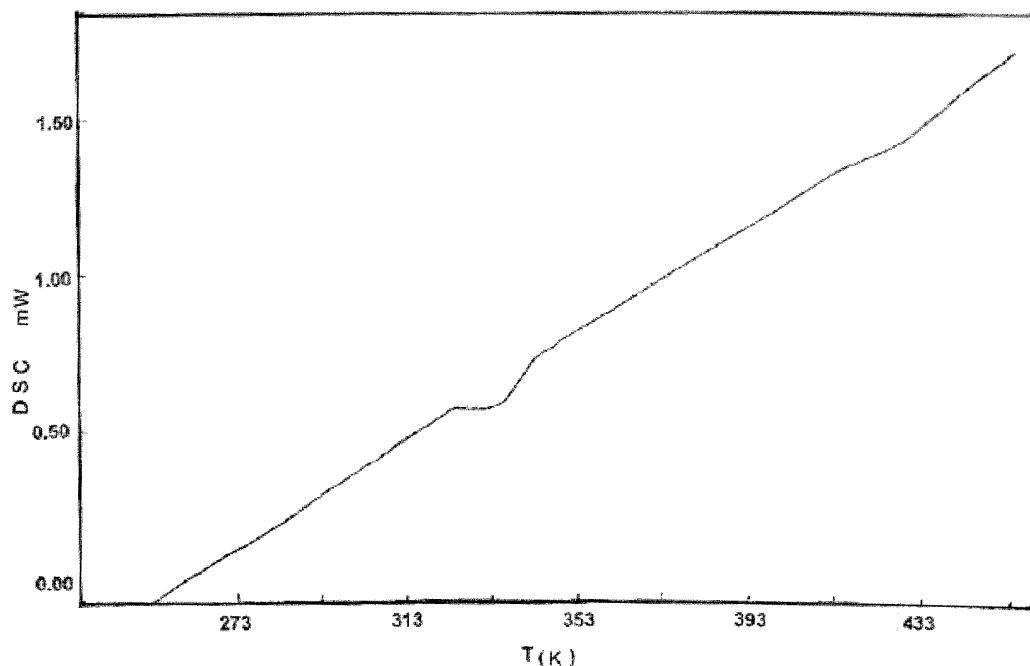


Fig. 2. DSC thermograph at 275–500 K of C3Cu.

Figure 2 shows the differential thermal scanning (DSC) thermograph in the temperature range 275–500 K, obtained while heating at a scanning speed of 10 °C/min. Two endothermic peaks are found at $T_1 = 333.5$ K and at $T_2 = 434.4$ K. The peak at T_2 is very broad and of small entropy, while the peak at T_1 has a λ -like shape with a tail on the high temperature side and a large enthalpy. The transition temperatures, enthalpies and entropies are listed in Table 3 along with the DSC results of the corresponding Mn and Cd salts for comparison [15]. The large enthalpy associated with the transition at T_1 suggests an order-disorder transformation.

3.2. Dielectric Response

Temperature Dependence

Figure 3a shows the temperature-dependent permittivity of C3Cu between room temperature and 445 K. Previous work in our laboratory showed that heating of alkylene-diammonium copper complexes to temperatures > 450 K results in an irreversible phase change [10]. The measurements were performed while heating in the frequency range 60 Hz–100 kHz. For clarity only a few selected frequencies are plotted. At temperatures below the transition temperature T_1 , de-

Table 3. Transition temperatures, enthalpies and entropies for $[(\text{CH}_2)_3(\text{NH}_3)_2]\text{MCl}_4$, M = Cu, Mn and Cd.

Compound	T (K)	ΔH (J/mol)*	ΔS (J/mol·K)**	Reference
$[(\text{CH}_2)_3(\text{NH}_3)_2]\text{CuCl}_4$	333.5	1272.4	3.82	this work
$[(\text{CH}_2)_3(\text{NH}_3)_2]\text{CuCl}_4$	434.4	771.525	1.53	this work
$[(\text{CH}_2)_3(\text{NH}_3)_2]\text{MnCl}_4$	305	500	1.7	[7]
$[(\text{CH}_2)_3(\text{NH}_3)_2]\text{MnCl}_4$	337	800	2.4	[7]
$[(\text{CH}_2)_3(\text{NH}_3)_2]\text{CdCl}_4$	374	1805	4.85	[15]

* Error in $\Delta H = \pm 150$ J/mol. ** Error in $\Delta S = \pm 0.4$ J/mol·K.

finned as region (IV), the permittivity is temperature- and frequency-independent. This is followed by a gradual rise associated with frequency dispersion up to $T = 380$ K identified as region (III). A plateau region (II) extends from 380 K up to $T = 429$ K ($f = 60$ Hz). The onset temperature shifts to higher values with increasing frequency. The increase in the permittivity associated with a plateau has been ascribed to rotation of dipoles [9, 10]. At $T \sim 429$ K a large increase in the permittivity occurs, leading to a peak at $T_2 \sim 433$ K, that decreases in intensity with increasing frequency in a manner similar to ferroelectric-like behavior [16]. $T_2 > 433$ K identifies region (I). This ferroelectric-like behavior is confirmed by the variation of ϵ' with temperature of a single crystal measured along the c -axis as seen in Figure 3b. Figure 3c shows the imaginary part of the

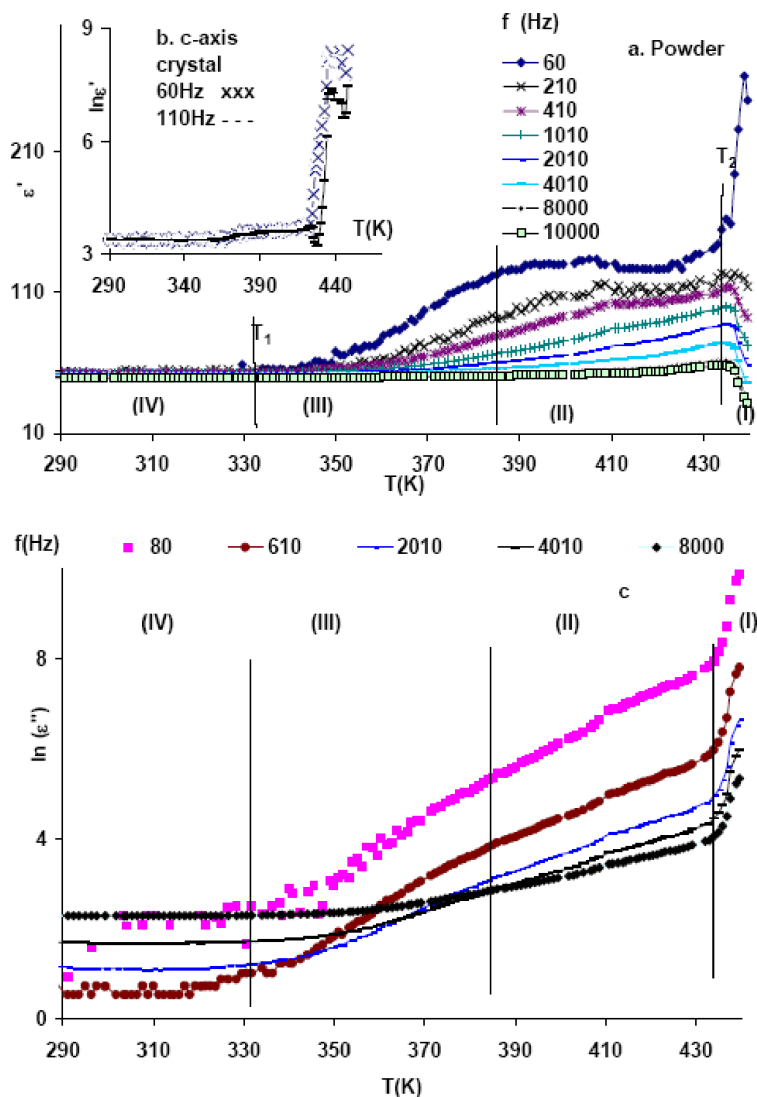


Fig. 3. (a) The real part of the permittivity vs. temperature between room temperature and 445 K of C3Cu. (b) The real part of the permittivity vs. temperature between room temperature and 445 K of C3Cu single crystal along the c -axis. (c) The imaginary part of the permittivity, $\ln \epsilon''$, as a function of the temperature at selected frequencies.

permittivity, $\ln \epsilon''$, as a function of temperature at selected frequencies. Four regions are also identified, where a temperature-independent behavior is noted up to $T \sim 340$ K and an anomalous increase in $\ln \epsilon''$ is observed near the transition temperature 433 K, and a change in the rate of increase of $\ln \epsilon''$ is found near $T = 380$ K.

Frequency Dependence

The dependence of the complex dielectric permittivity $\epsilon' + i\epsilon''$ on the frequency at several temperatures is presented in Figure 4. The real part of the permittivity ϵ' decreases with increasing frequency, however the rate of decrease is much faster for tem-

peratures $T \geq 434$ K (shown by dotted lines in Figure 4a). The variation of the imaginary part of the dielectric constant (ϵ'') on the log-log scale shown in Fig. 4b exhibits a relaxation peak in the high frequency range, but shows a linear dependence in the low and intermediate frequency ranges with slopes varying between 0.5 at $T = 350$ K to 0.86 at $T = 429$ K. For the high temperature phase $T > 434$ K, the relaxation peak vanishes and the slopes $(\ln \epsilon'')/(\ln \omega)$ for the high temperature phase are (1.0 ± 0.03) . Also one notices that the gradual decrease of ϵ'' with increasing frequency is shifting to lower frequencies as the temperature decreases. Such behavior reflects conductivity relaxation [17].

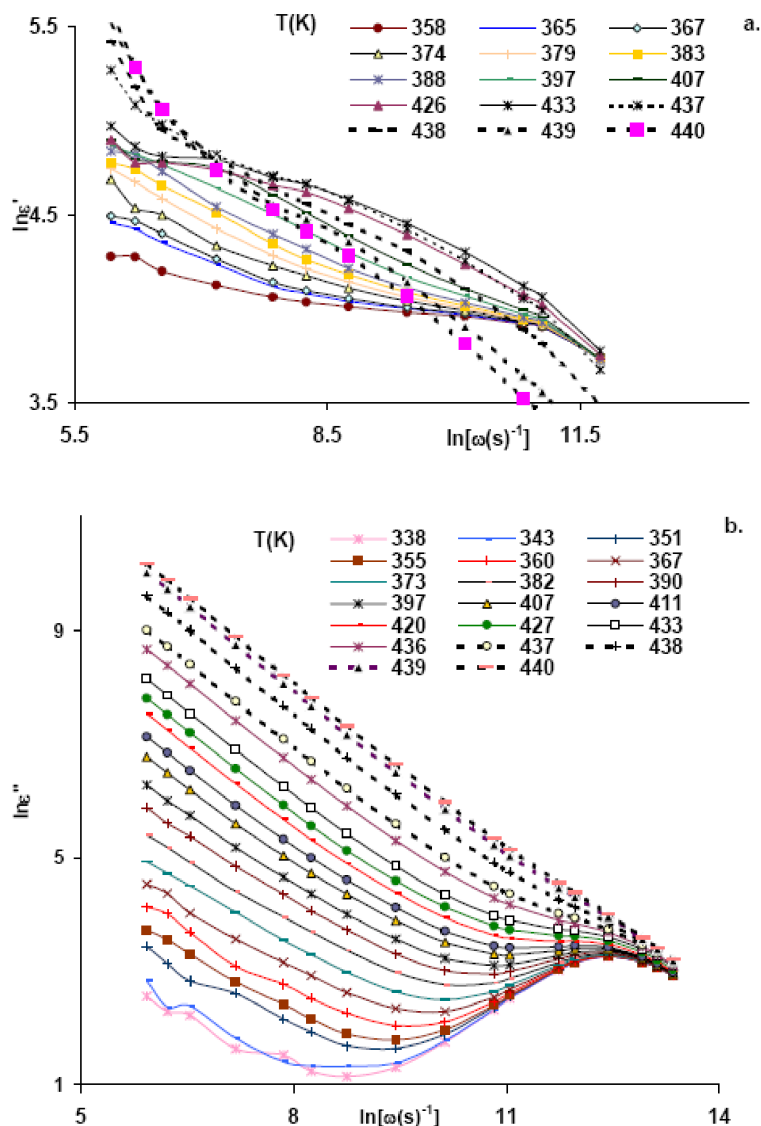


Fig. 4. (a) Real part of the permittivity, $\ln \epsilon'$, as a function of the frequency at selected temperatures. (b) The imaginary part of the permittivity, $\ln \epsilon''$, as a function of the frequency at selected temperatures.

3.3. Relaxation

Dipolar Relaxation

The frequency-dependent AC conductivity, $\sigma(\omega) = \epsilon'' \epsilon_0 \omega$, where ϵ_0 is the permittivity of free space and $\omega (= 2\pi f)$ is the angular frequency, at various temperatures is shown in Figure 5a. The conductivity shows dispersion at all frequencies for the different phases. There is a conductivity plateau in the lower frequency range at high temperatures, indicating mainly DC conductivity (σ_{dc}). Extrapolation of the conductivity in this region to $\omega = 0$ yields the DC conductivity (σ_{dc}), whose variation with temperature will be discussed be-

low. One also notices a crossover, at the frequency ω_p from the DC behavior to the dispersive AC conductivity, such that ω_p increases with temperature.

To get the dipolar relaxation, one has to subtract the DC conductivity contribution (σ_{dc}). The dielectric constant and the dielectric loss [$\epsilon''(\omega) - \sigma_{dc}/\omega \epsilon_0$] were fitted to the Cole-Cole function [18, 19]

$$\epsilon^* = \epsilon_\infty + (\epsilon_0 - \epsilon_\infty) / [1 + i(\omega \tau_d)^{(1-\alpha)}], \quad (1)$$

where ϵ_0 and ϵ_∞ are the low and high frequency dielectric constants, respectively. τ_d is the dielectric relaxation time of the dipoles and α is the Cole-Cole distribution parameter, having values between 0 and 1. The

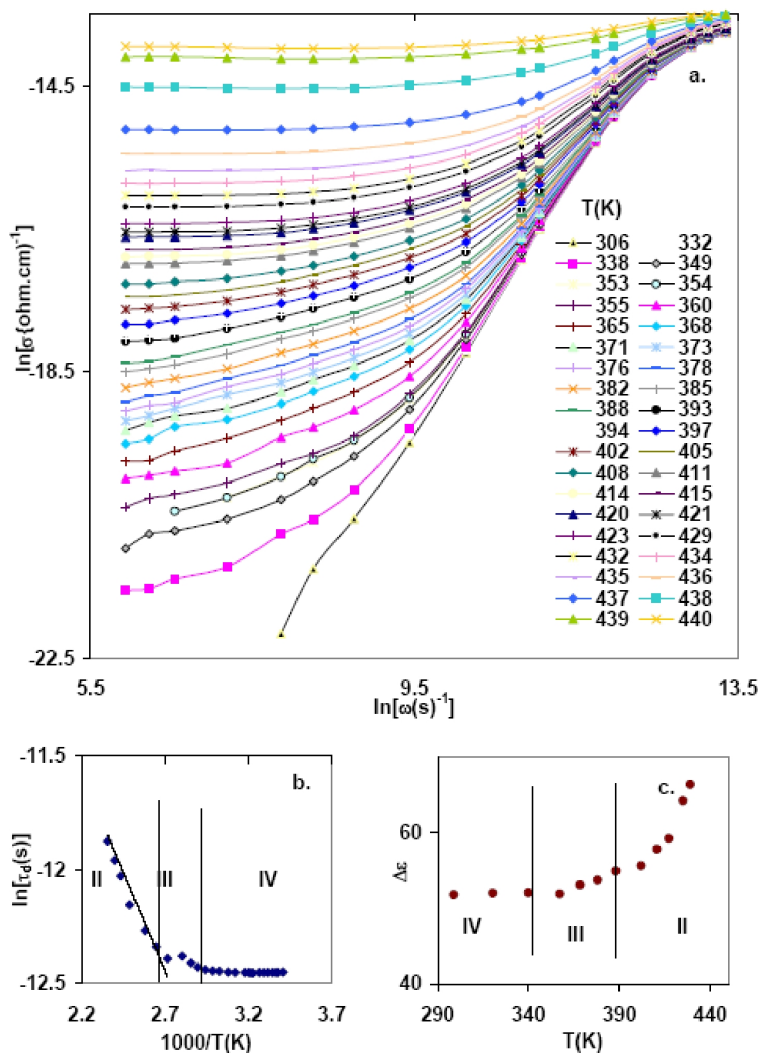


Fig. 5. (a) The dependence of the conductivity σ' on the frequency $\ln \sigma'$ vs. $\ln \omega$. (b) The dipolar relaxation $\ln \tau_d$ as a function of $1000/T$ (K). (c) The dielectric strength $\Delta\epsilon$ as a function of T (K).

parameters ϵ_∞ , ϵ_0 , τ_d , α and σ_{dc} were varied to get the best fit at different temperatures and frequencies. Dipolar relaxation times are plotted as $\ln \tau_d$ vs. $1000/T$ in Figure 5b. A nearly temperature-independent region is observed for $T \leq 340$ K (region IV) with an activation energy $\Delta E = 1.5 \cdot 10^{-3}$ eV. For the temperature range $380 \text{ K} > T > 429 \text{ K}$, region II, an activation energy $\Delta E = 9.2 \cdot 10^{-2}$ eV is found. Figure 5c also shows the dielectric relaxation strength $\Delta\epsilon = \epsilon_0 - \epsilon_\infty$ as a function of the temperature, which reflects a nearly temperature-independent behavior for region IV and a sharp rise of $\Delta\epsilon$ in region II. The value $\alpha = 0.17$ is small, indicating a slight deviation from Debye behavior in region II, and is almost zero in region IV.

Conductivity Relaxation

The electric modulus formalism M^* [20] will be used to get the conductivity relaxation, which is not due to dipolar relaxation in the bulk material. A plot of M^* vs. $\ln \omega$ is shown in Figure 6a. The S-shaped M' vs. $\ln \omega$ reflects the ionic nature of the material. Variation of the imaginary part M'' of the dielectric modulus with $\ln \omega$ shows bell-shaped peaks. The width of the peaks at half maximum (Δ) does not change appreciably with temperature, yet it is larger than the Debye peak (1.14 decades). The value obtained for Δ results in $\beta = 1.14/\Delta = 0.54$, indicating deviation from Debye characteristics [20]. It is also seen from Fig. 6a that the M'' maximum shifts to higher frequencies with in-

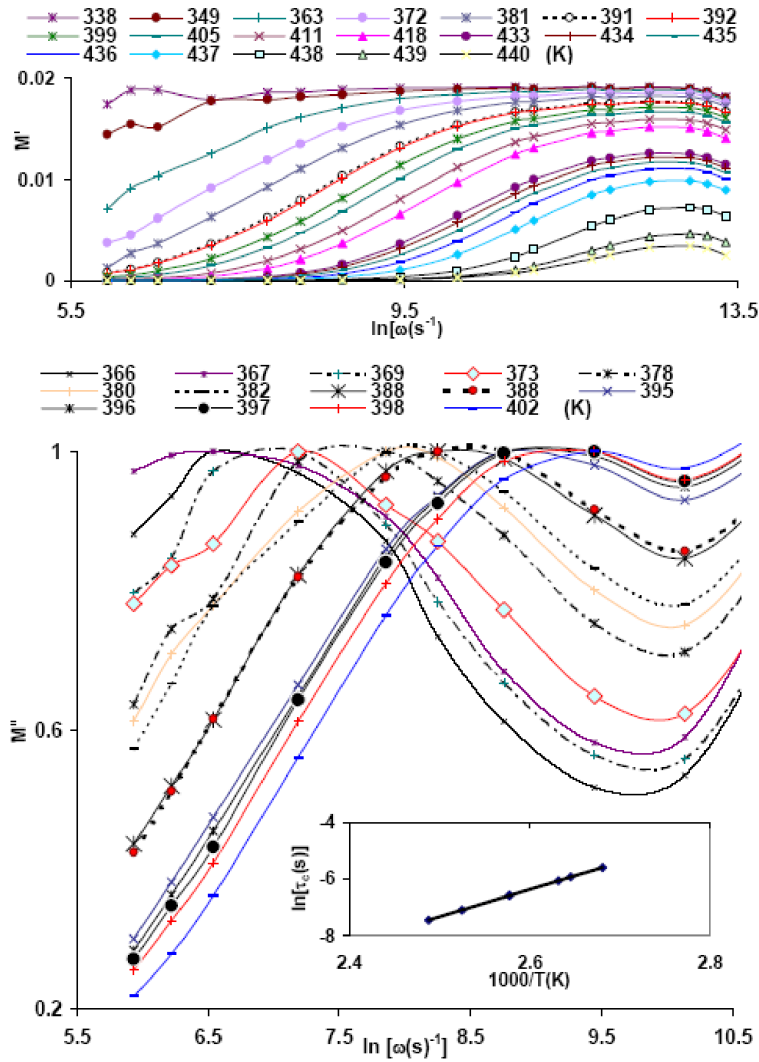


Fig. 6. The complex dielectric modulus $M^* = M' + iM''$ vs. $\ln \omega$. Insert: The conductivity relaxation $\ln \tau_c$ as a function of $1000/T(K)$.

creasing temperature, suggesting an activated behavior according to

$$\tau = \tau_0 \exp(\Delta E_c/kT), \tag{2}$$

where ΔE_c is the activation energy for the conductivity relaxation process and τ_0 is the high temperature limit of the relaxation time. The values of the activation energy and τ_0 found from the insert, Fig. 6b, is $\Delta E_c = 0.83$ eV, $\tau_0 = 2.19 \cdot 10^{-14}$ s. The value of the activation energy thus obtained lies in the range of values obtained from conductivity calculations, as will be shown below.

4. Transport Properties

4.1. Hopping Rate

Figure 7a depicts $\ln \sigma_{dc}$ as a function of the reciprocal temperature in the temperature range 380–437 K. The conductivity follows the Arrhenius relation [21]

$$\sigma_{dc} = A_0 \exp(-\Delta E/kT). \tag{3}$$

The equation indicates a thermally activated behavior with $\Delta E_I = (4.79 \pm 0.22)$ eV and $\Delta E_{II} = (1.21 \pm 0.01)$ eV for the regions I and II, respectively.

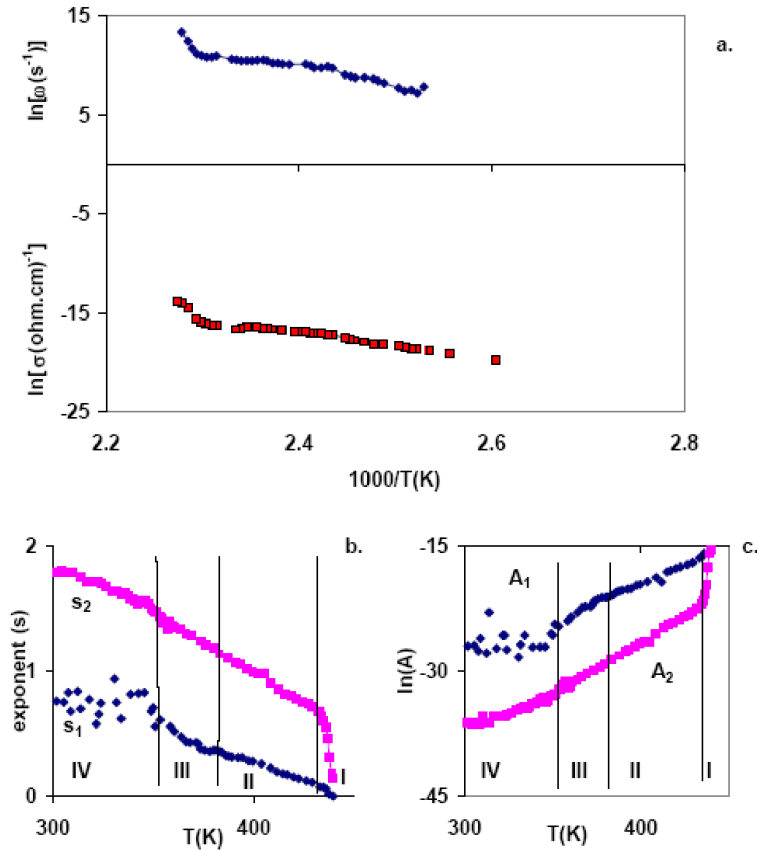


Fig. 7. (a) The hopping rate ω_p and the DC conductivity σ_{dc} as functions of reciprocal temperature $1000/T$. (b) The fitting parameters s_1 and s_2 as functions of the temperature. (c) The fitting parameters A_1 and A_2 as a functions of the temperature.

As mentioned above, the crossover frequency ω_p from the DC behavior to the dispersive AC conductivity is found to increase with temperature. Rolling *et al.* [22] defined the crossover frequency ω_p as

$$\sigma(\omega) = 2\sigma_{dc}, \text{ where } \omega = \omega_p. \quad (4)$$

The hopping rate was determined using (4).

Funggao *et al.* [23] related the DC conductivity σ_{dc} and the parameter A_0 to the ion hopping rate ω_p :

$$\sigma(\omega) = K\omega_p(1 + \omega/\omega_p)^n, \quad (5)$$

where $\sigma_{dc} = K\omega_p$, $A_0 = K(\omega_p)^{1-n}$. It is natural to expect the ion hopping rate to increase in a thermally activated manner, such that

$$\omega_p = \omega_0 \exp(-\Delta G/kT), \quad (6)$$

where ΔG is the free energy of the hopping process. Considering the concentration and temperature dependence of the mobile ions, one can compare the temperature dependence of the hopping rate with that of

the DC conductivity. The hopping rate, as obtained using (4), and the DC conductivity vs. $1000/T$ are shown in Figure 7a. The activation energies for the hopping rate were found to be (5.3 ± 0.5) eV and (1.5 ± 0.2) eV for the region I and II, respectively. These values are within the range found from the DC conductivity calculations. Hence the hopping rate and the DC conductivity have nearly equal slopes, suggesting no change in the concentration of the mobile ions within each region [23].

4.2. Frequency Dependence

The frequency dependence of $\sigma(\omega)$, shown in Fig. 5a, was fitted to the two terms power law

$$\sigma(\omega) = \sigma_{dc} + A_1\omega^{s_1} + A_2\omega^{s_2}. \quad (7)$$

The second term of (7) identifies the Jonscher regime [21], $0 < s_1 < 1$, which dominates at low frequencies and corresponds to translational motion of the mobile ions. The third term corresponds to the high

Region	T (K)	s_1	s_2	$\ln A_1$	$\ln A_2$
IV	$T < 340$	0.82	1.8	-27.99	-35.4 to -33.8
III	$340 < T < 380$	0.8-0.4	1.8-1.1	-27.74 to -21.8	-33.8 to -29.1
II	$380 < T < 429$	0.4-0.1	1.1-0.7	-21.8 to -17.05	-29.1 to -23.0
I	$T > 433$	0.1-0.002	0.65-0.15	-16.5 to -13.9	-22.5 to -15.5

Table 4. Values of the universal exponents and the pre-exponential factors for the different regions.

frequency dispersion region, where $1 < s_2 < 2$, that is associated with well localized hopping and/or reorientational motion. Values of the exponents s_1 and s_2 as well as the factors A_1 and A_2 are listed in Table 4, and their variations with temperature are shown in Fig. 7b and c, respectively.

The variation of the exponents s_1 and s_2 and the pre-exponential factors A_1 and A_2 reflect the changes in the conduction mechanism in the temperature range investigated, and the phase changes are expected to be manifested in their variations with temperature. One notices a gradual decrease of s_1 and s_2 with increasing temperature in the phases IV and III. Overlap large polarons (OLP) are known to show linearly decreasing s values up to a certain temperature, followed by an increase in s at higher temperatures [24, 25]. Thus the observed variation of the exponents s_1 and s_2 cannot be associated with OLP and the gradual variation of s_1 and s_2 with temperature depicted in Fig. 7b for the regions IV and III may qualitatively be associated with hopping over a barrier [25]. The anomalous changes in the pre-exponential factors A_1 and A_2 as well as the exponential factors s_1 and s_2 , particularly s_1 at $T \approx 333$ K and 429 K, are a result of the phase transitions occurring at these temperatures.

4.3. Temperature Dependence

The variation of $\ln \sigma_{ac}$ as a function of the reciprocal temperature is shown in Figure 8a. The results follow the Arrhenius relation with different activation energies depending on the temperature range. In phase IV, the conductivity is strongly dependent on the frequency and nearly temperature-independent with very low values of activation energies $\Delta E = 0.11$ eV ($f = 60$ Hz)–0.003 eV ($f = 10$ kHz), suggesting an extrinsic-type conductivity. In phase III the activation energy varies with frequency as seen in Fig. 8b and lies in the range 0.78 eV–0.04 eV, while in phase II it varies between 0.75 eV–0.028 eV. The conductivity is in the range $10^{-7} \Omega^{-1}\text{cm}^{-1}$ in both regions, indicating an ionic-type conduction. The variation of the activation energy with frequency is fitted to the equation

$$\Delta E = \Delta E_0 [1 - \exp(-\omega_0/\omega)]^\gamma. \quad (8)$$

Table 5. Bond distances (\AA) and angles ($^\circ$) of the room temperature phase [13].

	N...Cl	H...Cl	N-H...Cl
Non-bonding H11	3.213	2.34	171
Non-bonding H13	3.370	2.38	178
Bonding H12	3.271	2.58	170

The least squares fit to (8) yields $\Delta E_0 = (0.78 \pm 0.01)$ eV, $\omega_0 = (11023 \pm 805)$ Hz and $\gamma = (1.01 \pm 0.06)$ in region III, and $\Delta E_0 = (0.69 \pm 0.02)$ eV, $\omega_0 = (9436 \pm 306)$ Hz and $\gamma = (0.557 \pm 0.091)$ in region II.

As is known, a linear Arrhenius plot indicates that one charge carrier predominates, considering the unlikely coincidence of equal activation energies. The obtained Arrhenius plot shows curvature, indicating that different carriers contribute to the conductivity. Hence we suggest that in region III more than one mobile ion takes part in the conduction process. It is likely that protons as well as chloride ions contribute to the translational hopping. This is supported by the observed curvature and the change in the slopes at $T = 380$ K of s_1 and A_1 , as seen in Figs. 7b and 7c. It is possible that in region II a band-type conduction predominates.

The conductivity results are related to the structure of the material as follows:

The room temperature X-ray structure determination has indicated that the material is composed of chlorocuprate sheets that are puckered as a result of the hydrogen bonding to the propylene-diammonium chain. Cl^{35} NQR of the corresponding Mn and Cd salts has indicated the presence of two “bonding” chlorine sites due to corner sharing octahedra and “non-bonding” sites above and below the metal planes [6]. In phase III, two “non-bonding” and one bonding chlorine are involved in the NH_3 bonding scheme, resulting in a static puckering of the octahedra in opposite sense. In successive layers the puckering occurs alternately in opposite sense. At room temperature, phase IV has the same structure as phase II, however it is almost completely ordered. In phase III, the bonding scheme is different, where only one “non-bonding” chlorine and two “bonding” chlorines are involved, resulting in two equally probable orientations for the propylene-diammonium chains [7]. Table 5 lists the bond dis-

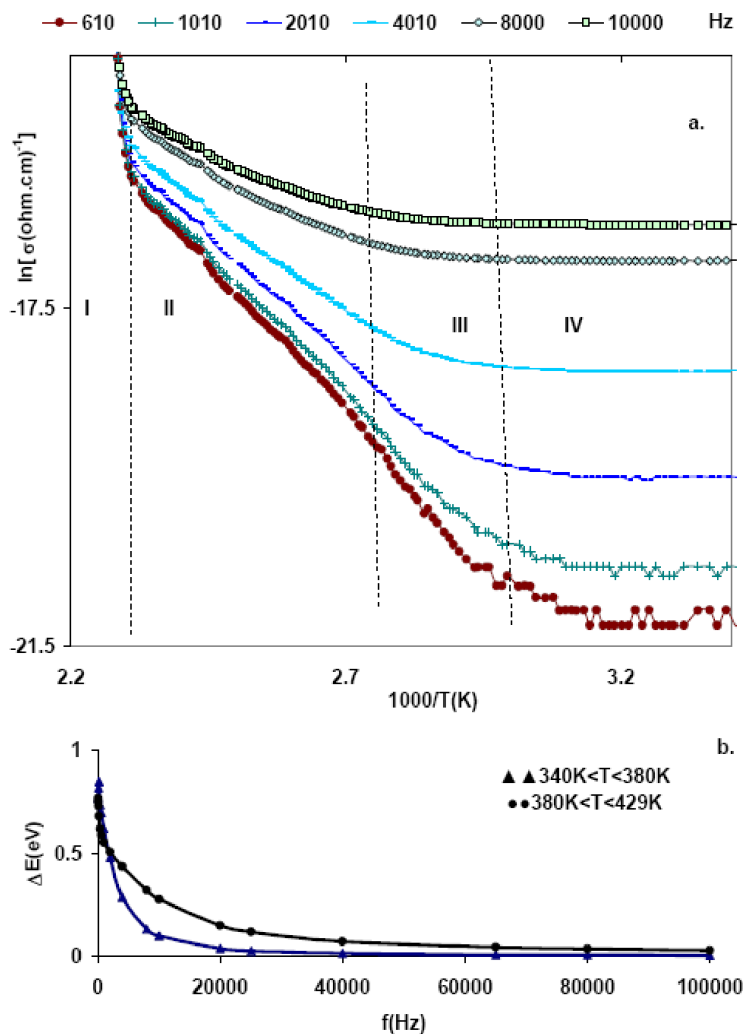


Fig. 8. (a) $\ln\sigma(\omega)$ as a function of $1000/T$. (b) The activation energy of the conductivity as a function of the frequency.

tances and bond angles of N...Cl and H...Cl and N-H...Cl.

Similar to the Mn and Cd salts, the phase transition of the corresponding Cu salt from phase IV to phase III should involve reorientational motion of the propylene chain associated with the breaking of one non-bonding H...Cl and the formation of a bonding H...Cl. Hence the conduction could be attributed to hopping of the protons and the "non-bonding" Cl ions among the increasing disordered vacant sites in this phase, as well as to the restricted reorientational motion of the organic moiety. The hydrogen bonding is statistically disordered, which still links the $[\text{CuCl}_4]^{2-}$ octahedra, but the bonding is much weaker than that at room temperature. Thus it is possible that both the proton and Cl ion hopping would contribute to the conduction in

region III. In regions I and II it is likely that band type conduction prevails.

5. Conclusion

The dielectric constant and differential thermal scanning of $[(\text{CH}_2)_3(\text{NH}_3)_2]\text{Cu}(\text{II})\text{Cl}_4$ indicates two structural phase transformations at $T_2 = 434$ K, associated with ferroelectric behavior, and an order-disorder transition at $T_1 = 333$ K. σ , T , ω of the AC conductivity suggest different conduction mechanisms, depending on the temperature regions. At high temperature, band-type conduction takes place, while hopping over a barrier predominates at low and intermediate temperatures.

- [1] A. Blake and W. Hatfield, *J. Chem. Soc. Dalton Trans.* **7**, 1725 (1979).
- [2] M. F. Mostafa, M. A. Semary, and M. M. A. Kader, *Physica B* **112**, 197 (1982).
- [3] M. A. Semary, M. F. Mostafa, and M. M. A. Kader, *Chem. Phys. Lett.* **97**, 741 (1983).
- [4] M. F. Mostafa, A. S. Atallah, and R. Emrick, *J. Appl. Phys.* **81**, 4135 (1997).
- [5] L. Snively, P. Seifert, K. Emerson, and J. Drumheller, *Phys. Rev. B* **20**, 2101 (1979).
- [6] R. Kind, S. Plesko, and J. Roos, *Phys. Status Solidi A* **47**, 233 (1978).
- [7] R. Kind, S. Plesko, P. Gunter, J. Roos, and J. Fousek, *J. Phys. Rev. B* **23**, 5301 (1981).
- [8] M. F. Mostafa, M. M. A. Kader, and S. S. Arafat, *Z. Naturforsch.* **57a**, 897 (2002).
- [9] M. F. Mostafa and A. A. Youssef, *Z. Naturforsch.* **59a**, 35 (2004).
- [10] M. F. Mostafa and S. A. El-Hakim, *Phase Transitions* **77**, 587 (2003).
- [11] R. Kind, *Ferroelectrics* **24**, 81 (1980).
- [12] H. V. Kanel and P. Wachter, *Physica B* **89**, 185 (1977).
- [13] D. Phelps, D. Losee, W. Hatfield, and D. Hodgson, *Inorg. Chem.* **15**, 3147 (1977).
- [14] M. F. Mostafa, M. M. A. Kader, A. S. Atallah, and M. El-Nimer, *Phys. Status Solidi A* **135**, 549 (1992).
- [15] M. Tello, M. Ariendiaga, and J. Fernandez, *Solid State Commun.* **24**, 299 (1977).
- [16] T. Mitsui, I. Tatsuzaki, and E. Nakamura, *An Introduction to the Physics of Ferroelectrics*, Gordon and Beach Science Publishers, New York 1977.
- [17] R. Neagu, E. Neagu, N. Bonanos, and P. Pissis, *J. Appl. Phys.* **88**, 7779 (2000).
- [18] K. Cole and R. Cole, *J. Chem. Phys.* **9**, 341 (1941).
- [19] S. Hazra and A. Ghosh, *Phys. Rev. B* **55**, 6278 (1997).
- [20] C. Moynihan, L. Boesch, and N. Laberg, *Phys. Chem. Glasses* **14**, 122 (1973).
- [21] A. K. Jonscher, *Dielectric Relaxation in Solids*, Chelsea Dielectric Press, London 1983, p. 340.
- [22] B. Rolling, K. Happe, K. Funk, and M. Ingram, *Phys. Rev Lett.* **78**, 2170 (1997).
- [23] C. Funggao, G. Saunders, Z. Wei, D. Allmond, M. Coutrone, and C. Mandanici, *Solid State Ionics* **109**, 89 (1998).
- [24] R. Elliott, *Adv. Phys.* **37**, 135 (1977).
- [25] A. R. Long, *Adv. Phys.* **31**, 553 (1982).